

Structure, Magnetism, and the Magnetocaloric Effect of MnFe_4Si_3 Single Crystals and Powder Samples

Paul Hering,[†] Karen Friese,^{*,†} Jörg Voigt,[†] Jörg Persson,[†] Nadir Aliouane,[‡] Andrzej Grzechnik,[§] Anatoliy Senyshyn,[⊥] and Thomas Brückel[†]

[†]Jülich Centre for Neutron Science JCNS-2 and Peter Grünberg Institute PGI-4, JARA-FIT, Forschungszentrum Jülich GmbH, 52425 Jülich, Germany

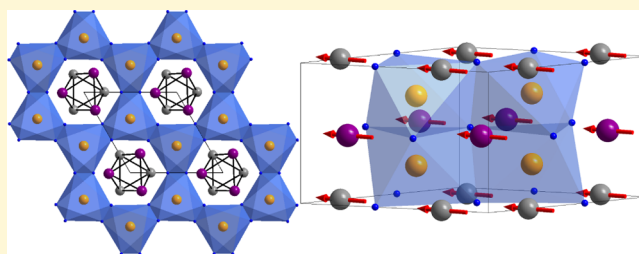
[‡]Paul Scherrer Institute, 5232 Villigen, Switzerland

[§]Institute for Crystallography, RWTH Aachen University, Jägerstr. 17-19, 52066 Aachen, Germany

[⊥]Heinz Maier-Leibnitz Zentrum, Technische Universität München, 85748 Garching, Germany

S Supporting Information

ABSTRACT: Magnetic and structural properties of high quality magnetocaloric MnFe_4Si_3 single crystals are investigated macroscopically and on an atomic scale. Refinements of combined neutron and X-ray single crystal diffraction data introduce a new structural model in space group $P\bar{6}$ characterized by partial ordering of Mn and Fe into layers perpendicular to c on one of the transition metal sites. A second transition metal site is exclusively occupied by iron. MnFe_4Si_3 has a phase transition to a ferromagnetically ordered phase at approximately 300 K and displays a strong anisotropy of the magnetization and the magnetocaloric effect with the easy axis of magnetization in the a,b -plane. This is confirmed by a refinement of the magnetic structure in the magnetic spacegroup Pm' , which shows that the spins on the sites with mixed occupancy of Mn and Fe are aligned in the a,b -plane. A significant magnetic moment for the site exclusively occupied by iron could not be refined. The thermal evolution of the lattice parameters exhibits an anisotropic behavior and clearly reflects the onset of magnetic ordering. A comparison of the ordered moment and the effective paramagnetic moment hints toward itinerant magnetism in the system.



INTRODUCTION

Magnetic cooling offers an opportunity of an energy savings of about 20–30% compared to conventional vapor compression technology and does not use any ozone depleting gases or other environmentally hazardous refrigerants.¹ The magnetic refrigeration cycle makes use of the magnetocaloric effect, that is, the temperature change upon adiabatic magnetization/demagnetization.² The entropy change in magnetocaloric materials shows a peak at temperatures corresponding to magnetic phase transitions, leading to a comparably large temperature change to keep the total entropy constant.

Compounds in the series $\text{Mn}_{5-x}\text{Fe}_x\text{Si}_3$ show magnetocaloric effects at different temperatures depending on the individual composition.³ On the basis of X-ray and neutron powder diffraction studies at 293 and 77 K, it was postulated that all compounds in the series crystallize in the space group $P6_3/mcm$ in the investigated temperature range.⁴ Two sites M1 (Wyckoff position 6g) and M2 (Wyckoff position 4d) are occupied by Mn and Fe in different ratios depending on the parameter x . The M1 atoms are interconnected to form distorted octahedra. These octahedra share common triangular faces and form chains of composition $\infty[(\text{M1})_3]$ along the c -direction. The M2 site is surrounded by six silicon atoms at distances of

approximately 2.4 Å in the form of a distorted octahedra. Neighboring $[\text{M2Si}_6]$ octahedra share triangular faces and also form infinite chains of composition $\infty[(\text{M2})\text{Si}_3]$ along the c -direction.^{4,5}

On the basis of magnetization measurements on polycrystalline material, a variety of magnetic phase transitions were identified^{3,5,6} in the temperature range between 25 and 400 K. Of particular interest is MnFe_4Si_3 as its ferromagnetic ordering sets in at approximately 300 K.^{3,5,6} Rietveld refinements of the magnetic structure were carried out in the magnetic space group $P6_3/mc'm'$ and resulted in an alignment of the spins parallel to the $[001]$ -direction. Furthermore, a two-step spin ordering process was assumed where the two metal sites M1 and M2 have different ordering temperatures and magnetic moments.⁵

The magnetic entropy change deduced from the hysteresis loops measured on polycrystalline samples using the Maxwell relation is about 3 J/kg K at a field change from 0 to 2 T and about 4 J/kg K for a field change from 0 to 5 T.^{5,7} Although this

Received: August 14, 2015

Revised: October 5, 2015

Published: October 5, 2015

change is only modest, the material has other advantageous key properties that make it an interesting candidate for further optimization, for example, through doping with other elements. The compound consists of nontoxic, abundant, and cheap elements^{8,9} and is less fragile than competing materials, which can be of major advantage during molding or processing. In addition, it is straightforward to grow large single crystals of MnFe_4Si_3 , unusual for magnetocaloric materials, which frequently only exist in polycrystalline form.

We decided to reinvestigate the thermal expansion, magnetic properties, the crystal and magnetic structure of MnFe_4Si_3 . In contrast to the studies performed earlier, we had large single crystals of the material available. This allowed us not only to perform direction-dependent measurements of the magnetization, but also opened the way for detailed investigations of the crystal and magnetic structure using single crystal X-ray and neutron diffraction. Since studies of single crystalline magnetocaloric materials are scarce, our study provides important insights on the role of anisotropy in magnetocaloric materials in general.

EXPERIMENTAL SECTION

For the synthesis of the polycrystalline samples of MnFe_4Si_3 , elementary manganese (Aldrich, 99.99%), iron (Aldrich, 99.99%), and silicon (Aldrich, 99.99%) were used. The manganese pieces were etched prior to the synthesis in hydrochloric acid to obtain a clean unoxidized surface. All raw materials were heated under vacuum to remove remaining impurities, especially surface water. The elements were mixed in stoichiometric ratios and melted in argon atmosphere by induction heating in a levitation cold crucible.¹⁰ The resulting product was cooled and heated four times to ensure maximum homogeneity of the sample. Single crystals were grown from the polycrystalline material using the Czochralski method¹¹ in an aluminum oxide crucible with a tungsten crystal as seed crystal. The final single crystal had a diameter of about 8 mm and was cut by spark erosion into two large single crystal samples (ca. 2.5 mm × 2 mm × 2 mm, 0.0538 g and ca. 1.5 mm × 1.5 mm × 1 mm, 0.00972 g). Part of the remaining pieces (≈ 10 g) were ground to obtain samples for the powder diffraction experiments, while a small single crystal (200 μm × 200 μm × 200 μm) was selected for X-ray single crystal diffraction.

The smaller single crystal (0.00972 g) was cut perpendicular to the hexagonal [100], [120], and [001]-direction for the magnetization measurements, which were carried out with a Quantum Design MPMSXL system. Three data sets were collected with the applied external magnetic field being oriented perpendicular to the pre-cut faces. For the data sets with the field along the [100]- as well as the one with the field along the [120]-direction, isothermal magnetization curves have been recorded in the field range $-2T < \mu_0 H < 2T$ at different temperatures between 50 and 390 K. The corresponding isothermal magnetization measurements with an applied external field along the [001]-direction were performed for a field range from $-4T < \mu_0 H < 4T$ using the same temperature points. One additional high field isothermal magnetization curve was measured with a Cryogenics Ltd. CCMS system in a field range from $-14T < \mu_0 H < 14T$ at 50 K. Temperature dependent magnetization measurements on the same sample were performed with a Quantum Design PPMS DynaCool system. They were measured in 400 steps while sweeping the temperature with a rate of 1 K/s in a range from 310–700 K with a magnetic field of 0.005 T applied perpendicular to the [001]-direction. In addition, three temperature dependent magnetization measurements were performed with a magnetic field of 0.01 T applied perpendicular to the [001]-, the [120]-, and the [100]-direction while sweeping the temperature with a rate of 3 K/s in a range from 250–350 K.

The neutron powder diffraction data were collected at the high resolution powder diffractometer SPODI¹² of the beamline 8a at the Maier Leibnitz Zentrum (MLZ) in Garching, Germany. About 10 g of

polycrystalline material was measured in a vanadium sample holder. Temperature-dependent measurements were performed with an MLZ standard cryo-furnace from the base temperature of 4 K to a maximum temperature of 470 K. We took 40 diffraction patterns and illuminated the sample for 30 min. Two data sets at 4 and 380 K have been measured with higher statistics (3 h). The used neutron wavelength was $\lambda = 1.548$ Å. The instrumental geometry as well as the preprocessing of the data, which is needed to obtain the one-dimensional data from the detector tubes for further analysis, is described in detail in ref 12.

For the X-ray single crystal diffraction, an Agilent Supernova with $\text{MoK}\alpha$ radiation was used. A total of 972 frames was measured at the temperatures 425 K, 380 K, 335 K, 290 K, 245 K, and 200 K using a Cryojet HT cryo-furnace from Agilent with a temperature stability of 0.1 K. The data were reduced with the software CrysAlisPro from Agilent.¹³ For the empirical absorption correction, the crystal shape was approximated by 20 faces, which were optimized with the program X-shape.¹⁴ The total number of observed reflections was ~ 4500 at all temperatures.

Neutron single crystal diffraction measurements were performed at TRICS (Beamline R42) at the SINQ spallation source of the Paul Scherrer Institute.¹⁵ The beamline was equipped with a four circle goniometer in Euler geometry, and we used a ³He-point-detector. The large single crystal (2.5 mm × 2 mm × 2 mm) was mounted on an aluminum pin. A total number of 425 reflections were measured at temperatures of 380 and 200 K with ω -scans at a wavelength of $\lambda = 1.178$ Å using an APD Cryogenics cryostat. All reflection profiles were integrated with a Gaussian function. Further details concerning the X-ray and neutron single crystal measurements are provided in Tables 2–4 as well as in the deposited CIF-files.

REFINEMENTS

LeBail Refinements of the Neutron Powder Data.

Starting from the lowest temperature, LeBail refinements¹⁶ of the neutron powder data were performed with the program JANA2006.¹⁷ The background was defined manually, and a pseudo-Voigt-function with five free parameters was used for profile fitting. The zero shift was refined, and a Simpson correction¹⁸ to describe the slightly asymmetric peak shape was applied. Two additional phases had to be introduced: aluminum resulting from the experimental setup and a binary iron manganese phase ($\text{Fe}_{0.5}\text{Mn}_{0.5}$), which was present as a minor impurity phase ($<0.5\%$). Final wR_p values are in the range from 3–4.5% at all temperatures. A representative fit is shown in Figure 1.

Refinements of the Single-Crystal Data. For the structure refinement of the data sets at 380 K, which were carried out with the program Jana2006,¹⁷ both the neutron and the X-ray data were taken into account simultaneously. An

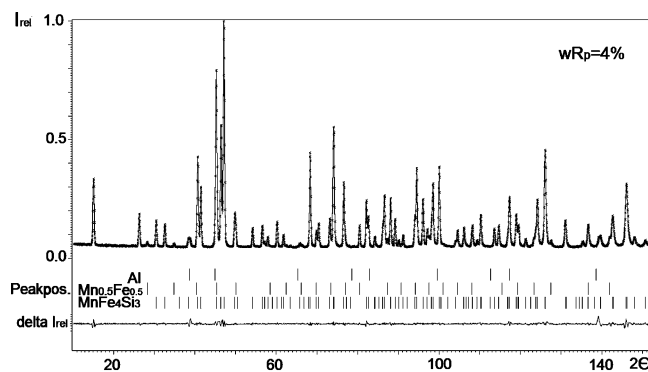


Figure 1. Representative LeBail-fit of a neutron powder diffraction diagram of MnFe_4Si_3 measured at SPODI (MLZ, Garching) at 4 K.

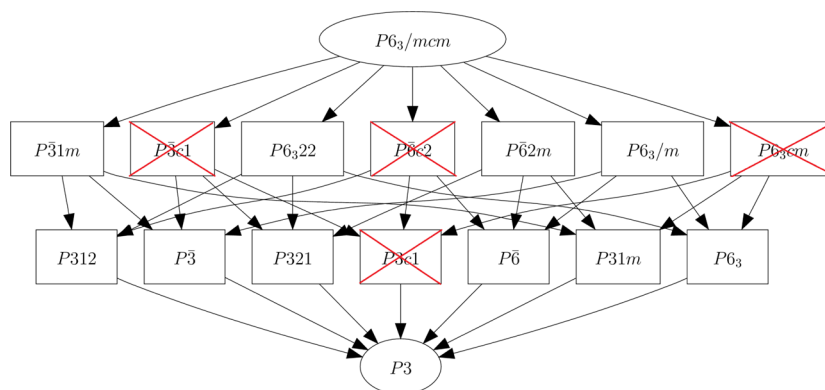


Figure 2. Group–subgroup relationships between $P6_3/mcm$ and $P3$. Subgroups including the c -glide plane could be excluded as the corresponding extinction rules are not observed. Drawn with the program SUBGROUPGRAPH.¹⁹

inspection of the X-ray data showed extinction rules in accordance with the space group suggested in the literature ($P6_3/mcm$). However, for the neutron diffraction data, a series of reflections violating the extinction rules for the c -glide plane were observed (61 observed reflections). These observations can be readily understood due to the fact that the X-ray scattering factor curves for Fe and Mn are very similar, yet the neutron scattering lengths for both atoms are very different. Any additional ordering of Mn/Fe is therefore likely to be seen in the neutron, but not necessarily in the X-ray data. Because of the observed systematic absence of violations, several trial refinements in the hexagonal and trigonal subgroups of $P6_3/mcm$ (Figure 2), which do not contain the c -glide plane, were carried out. Starting models were deduced from the model in $P6_3/mcm$ on the basis of group–subgroup relationships.

Rotational symmetry elements lost in the respective symmetry reductions were taken into account as twinning elements. Hamilton tests²⁰ of the different models showed the space group $P\bar{6}$ to be the best choice. The sums of the occupancies for the mixed Mn/Fe sites were restricted to the ideal values in the final model, as trial refinements showed no significant deviations. Mn and Fe on the mixed occupancy sites were found to have slightly different coordinates in the difference Fourier based on the neutron single crystal data and were refined accordingly. Anisotropic displacement parameters of Mn/Fe on these sites were restricted to be equal. Structure refinements of data corresponding to temperatures where only X-ray data were available were carried out in space group $P6_3/mcm$, which can be regarded as an average structure of the model on $P\bar{6}$. Occupancies of the mixed sites were fixed to the ones deduced from the results at 380 K. The combined neutron and X-ray data sets were used to refine the nuclear and magnetic structures of $MnFe_4Si_3$ at 200 K. Possible magnetic space groups were deduced on the basis of the irreducible representations of the space group of the nuclear structure using the corresponding option provided in Jana2006.²¹

Details of all the refinements, atomic coordinates, anisotropic displacement parameters, and refined magnetic moments are given in the Supporting Information. Further details of the crystallographic investigations can also be obtained from the Fachinformationszentrum Karlsruhe, D-76344 Eggenstein-Leopoldshafen, Germany, on quoting the depository numbers CSD 429968–429975.

RESULTS AND DISCUSSION

Macroscopic Magnetization Measurements. We could for the first time perform direction dependent magnetization measurement on $MnFe_4Si_3$. The measurements confirm the temperature of the magnetic transition observed earlier.^{3,5,6} In the measured temperature range, the hysteresis loops measured with the magnetic field directed parallel and perpendicular to the crystallographic c -axis of the compound show a pronounced anisotropy of the magnetic response, which has not been described before (Figure 3; further hysteresis loops are

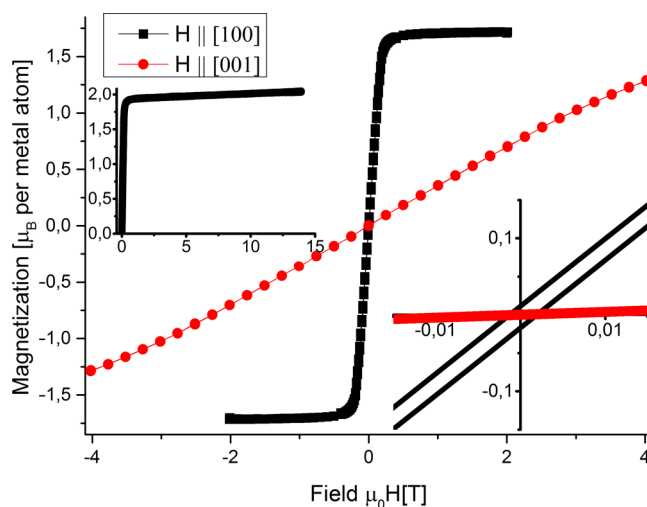


Figure 3. Hysteresis loops of $MnFe_4Si_3$ showing the magnetization as a function of the applied magnetic field at 50 K. The inset (lower right) is a close-up of the region around 0 T for both curves. The inset (upper left) shows the magnetic response along the [100]-direction up to 14 T at 40 K. The line widths correspond to the size of the standard deviations.

provided in the Supporting Information). Hysteresis loops with the field \parallel [100] and \parallel [120] are identical throughout the measured temperature region within the experimental errors and show ferromagnetic characteristics with a small opening of the hysteresis loops with a coercive field of 1 mT below temperatures of about 300 K. The magnetization rapidly reaches about $1.7(1) \mu_B$ per metal atom at a field of 0.5 T at a temperature of 50 K. At higher fields, a slightly increasing linear behavior up to 14 T reaches no clear saturation (see inset in Figure 3).

Hysteresis loops measured with the field along the [001]-direction show a different behavior (Figure 3): the magnetization increases more slowly with increasing field, and up to 4 T, no clear saturation is reached; within the accuracy of the measurement, an opening of the hysteresis loop is not detected (see inset in Figure 3). These observations strongly suggest that the directions within the a,b -plane are the easy axes of magnetization, while the c -direction is the hard magnetization axis of MnFe_4Si_3 . This is in clear contrast to the earlier results obtained on polycrystalline material, which assumed that the magnetic spins order parallel to the [001]-direction.^{3,5} The temperature dependent magnetic response for a field of 0.01 T applied in the directions parallel to [100] and [120] (Figure 4)

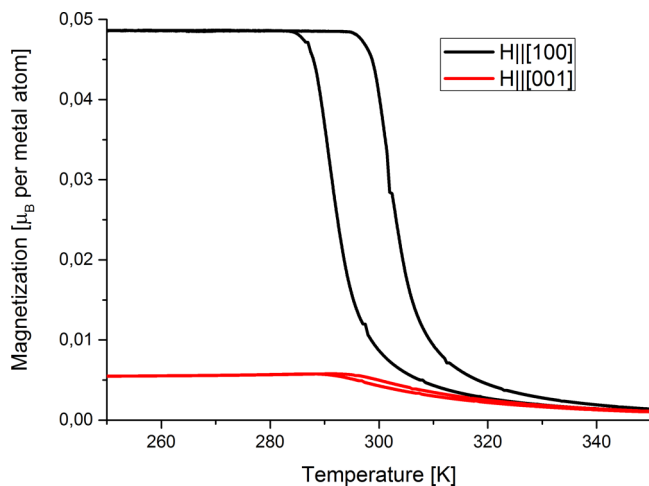


Figure 4. Hysteresis loops of MnFe_4Si_3 showing the magnetization as a function of the temperature at 0.01 T. The line widths correspond to the size of the standard deviations.

is within errors identical and shows a clear hysteretic behavior of about 10 K along these directions. This indicates the presence of latent heat and confirms that the thermodynamic character of the ferromagnetic transition is of first order. An applied field of 0.01 T in the direction parallel to [001] causes a much smaller hysteretic behavior of the temperature-dependent magnetization of only about 1–2 K.

As can be seen from Figure 5, the magnetocaloric effect also shows a significant anisotropy. The isothermal entropy change ΔS was calculated numerically from Maxwell's relation:

$$\Delta S_m(T, \Delta B) = \sum_i \frac{M_i(T'_i, B_i) - M_i(T_i, B_i)}{T'_i - T_i} \Delta B_i \quad (1)$$

Although Maxwell's relation is only strictly valid for materials with a second-order transition, it still provides a good approximation for materials with a first-order magnetic transition.²² With an applied field along the a -axis, the magnetic entropy change has a maximum of -2.90 J/kg K for a field change of 2 T. This value is slightly higher than the values observed for polycrystalline samples (≈ -2 J/kg K at a field change from 0 to 2 T and ≈ -4 J/kg K for a field change from 0 to 5 T^{5,7}). If a magnetic field of 2 T is applied parallel to the c -axis, the entropy change is considerably smaller (approximately -1.3 J/kg K; see Figure 5). These observations demonstrate that the MCE in this compound is clearly dominated by the magnetic moments aligned in the a,b -plane.

Figure 6 shows the inverse molar magnetic susceptibility of MnFe_4Si_3 at an applied field of 0.005 T along the [100]-direction. The linear paramagnetic region above 550 K follows the Curie–Weiss law. The resulting Curie-constant is $C_m = 6.7(1) \times 10^{-5} \text{ m}^3 \text{ K/mol}$, the Debye-temperature is 366(5) K, and the effective magnetic moment per transition metal atom is $2.9(4) \mu_B$. Standard deviations on these values cover the statistical errors as well as systematic errors of the setup and data treatment. According to earlier Mössbauer and magnetization measurements,²³ the magnetic moments of MnFe_4Si_3 were assumed to be partly itinerant and partly localized. A possible indication for the itinerant nature of the magnetic properties can be obtained from the Rhodes–Wohlfarth plot.²⁴ The ratio of the magnetic moments obtained from the Curie–Weiss law (q_c) to the moment obtained from low temperature saturation magnetization (q_s) as obtained from our measurements is $q_c/q_s = 1.7$. This value indeed lies on the branch of the Rhodes–Wohlfarth plot for materials with itinerant magnetism and thus agrees with the earlier assumptions in ref 23.

Lattice Parameter as a Function of Temperature. The lattice parameter and the unit cell volume as a function of temperature are shown in Figure 7 (absolute values of the

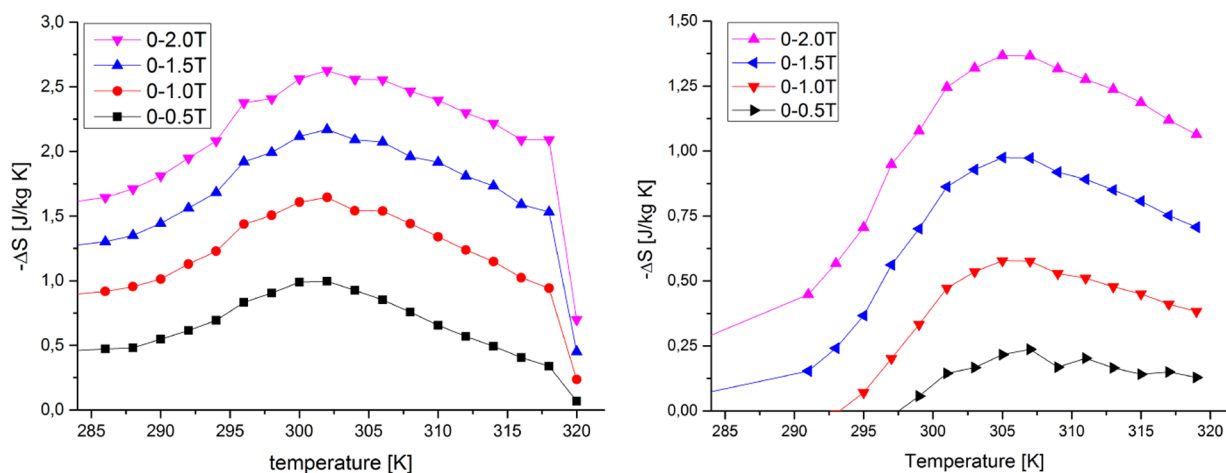


Figure 5. Selected curves showing the isothermal entropy change ΔS , which serves as a measure for the MCE. Calculated from Maxwell's relation on the basis of the measured magnetic hysteresis loops (see Supporting Information) with an applied field along the [100]-direction (left) and along the [001]-direction (right).

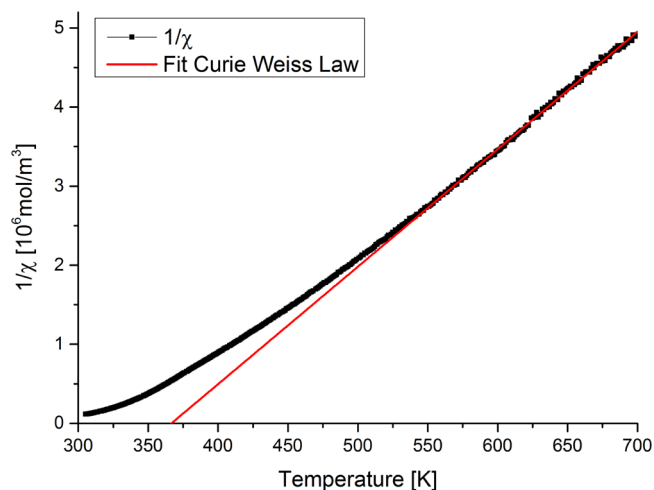


Figure 6. Inverse magnetic molar susceptibility as a function of temperature. The red line describes the fit to the data based on the Curie–Weiss law (applied field of 0.005 T along the [100]-direction). The corresponding errors are smaller than the symbols.

lattice parameters are listed in the [Supporting Information](#)). Lattice parameters at 300 K ($a = 6.80572(22)$ Å and $c = 4.72965(16)$ Å) are in good agreement with earlier data.^{4,5} The wide temperature range studied by us clearly reflects the response of the lattice parameter to the magnetic ordering. The a -lattice parameter decreases monotonically in the temperature region from 500–310 K. Below 300 K, it shows a pronounced increase, which coincides with the beginning of magnetic ordering again hinting at the first-order character of the phase transition. At ~ 250 K, it starts to slightly decrease again. (In a narrow temperature range around 20 K, an anomaly with a

sharp rise and lowering of the a and c lattice parameters can be noted. As the structural origin of this anomaly is unknown, this requires further investigation, which is, however, out of the scope of this article.) The c -lattice parameter decreases in the full temperature range from 480–20 K.

The bottom right of [Figure 7](#) shows the normalized values of the lattice parameters and the unit cell volume. The compound has strong anisotropic thermal expansion, as the changes in the c -lattice parameter (~ 0.03 Å in the measured temperature range) are five-times higher than those of the a -lattice parameter (~ 0.006 Å). The anisotropic thermal expansion is nicely reflected in the Guinier simulation ([Figure 8](#), this pseudo three-dimensional simulation was obtained by stacking the diffraction patterns using the individual temperatures of the measurements as y -axis; the diffracted intensity is encoded in a color code) by the splitting and “bending” of the observed powder lines in the high θ -range.

Structure of MnFe_4Si_3 at 380 K. The simultaneous refinement using both X-ray and neutron single crystal diffraction data sets for 200 and 380 K leads to an advanced model of the crystal structure and magnetic structure compared to the ones obtained from powder data. Our refinements show the symmetry of the compound to be lower than stated earlier. The symmetry reduction from $P6_3/mcm$ to $P\bar{6}$ is mainly due to a partial ordering of Fe and Mn on the sites with mixed occupancy, which is not in accordance with a c -glide plane. Because of the limited contrast, the partial ordering of Mn and Fe is not noticeable in the X-ray data, but it is clearly reflected in the neutron data. While in the higher symmetrical space group $P6_3/mcm$, three symmetrically independent sites are occupied in the structure (M1 at WP position 6g; M2 at WP 4d; Si at WP 6g); these Wyckoff positions are split in space group $P\bar{6}$, and six symmetrically independent sites exist (M1a/

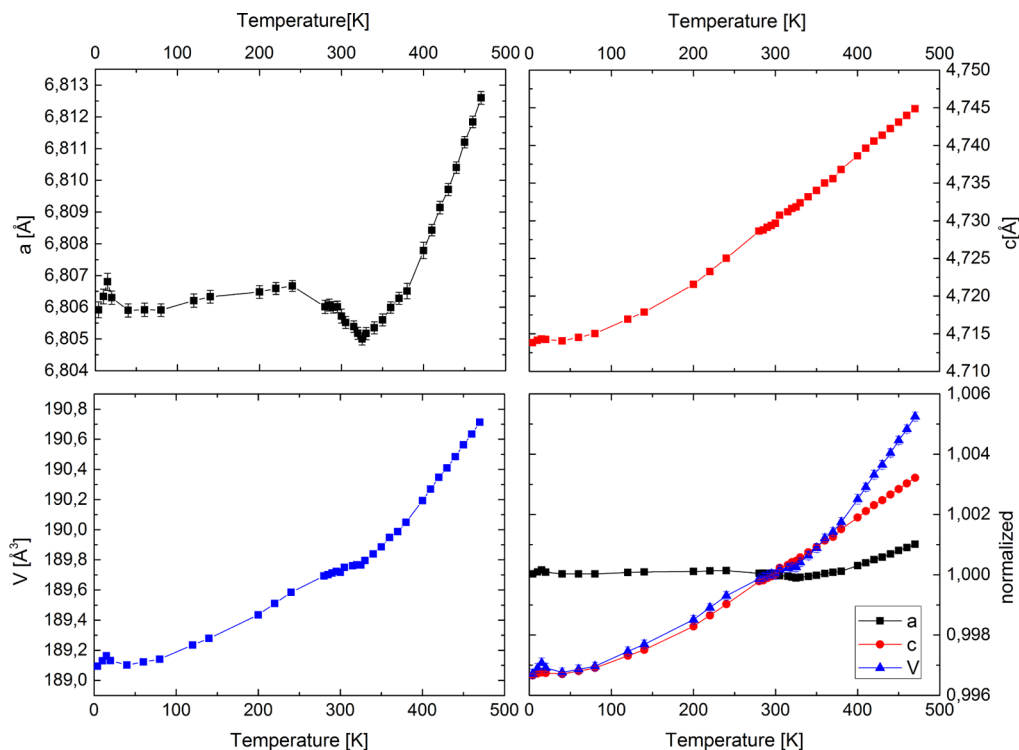


Figure 7. Lattice parameter and unit cell volume of MnFe_4Si_3 as a function of temperature. The figure at the bottom right shows the normalized lattice parameter and unit cell volume using the values at 300 K for normalization. Error bars are shown if the error exceeds the size of the symbols.

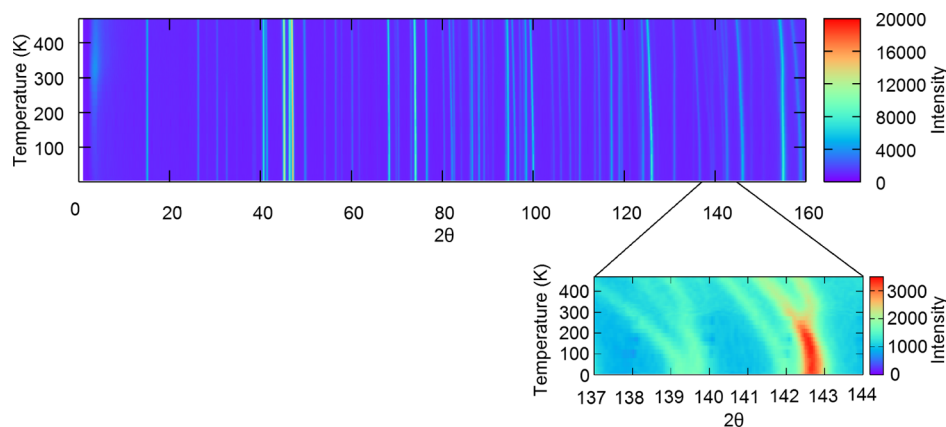


Figure 8. Guinier simulation based on the neutron powder diffraction data of MnFe_4Si_3 measured at SPODI, MLZ, Garching, Germany. The section in the lower right shows the splitting and “bending” of the observed powder lines in the high θ -range (137° – 144°), which can be attributed to anisotropic thermal expansion.

M1b, WP 3j/3k; M2a/M2b, WP 2h/2i; Si1a/Si1b, WP 3j/3k). According to the structural model in $P6_3/mcm$ published in ref 4, most of the Mn is incorporated into the M1 site, and the M2 site is nearly exclusively occupied by Fe.⁴ In the advanced model in $P\bar{6}$, the M1a- and M1b-sites show slightly different occupancies by Mn and Fe: M1a, 37.6(2) %Mn and 62.8(2) %Fe; and M1b, 27.7(7) %Mn and 72.3(7) %Fe (Figure 9). This

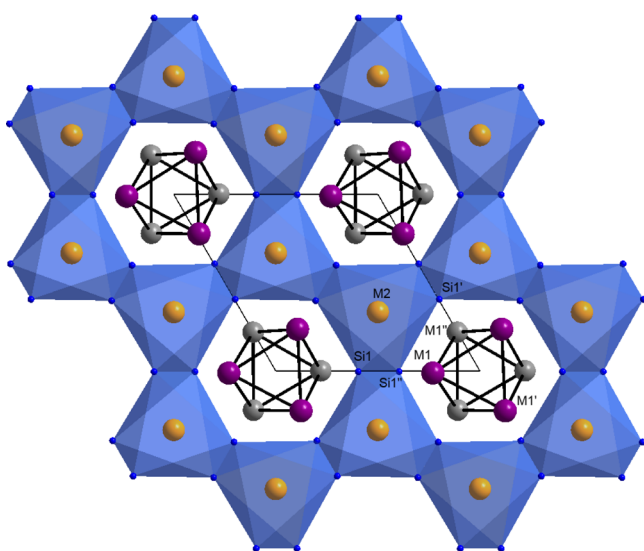


Figure 9. Projection of the structure of MnFe_4Si_3 in space group $P\bar{6}$ at 380 K along the $[001]$ -direction. Sites occupied by Mn and Fe are shown in magenta (M1a) and gray (M1b); sites exclusively occupied by Fe are shown in orange; Si atoms are shown in blue. Magenta and gray sites are in different layers along the $[001]$ -direction. Shortest distances between M1a and M1b sites are indicated in black, and $[\text{FeSi}_6]$ -octahedra are indicated in blue. Labels of atoms correspond to the distances in Figure 11.

indicates a partial ordering of the Mn and Fe, which are incorporated into the M1Si_6 -octahedra into different layers (Figure 10). In addition, differences in Fourier syntheses and the subsequent refinement of the resulting positions showed that Mn and Fe occupy sites, which are 0.092(5) Å (Mn1a/Fe1a) and 0.164(5) Å (Mn1b/Fe1b) apart. According to our refinement, the M2a/M2b sites on the other hand are exclusively occupied by Fe. The overall stoichiometry from

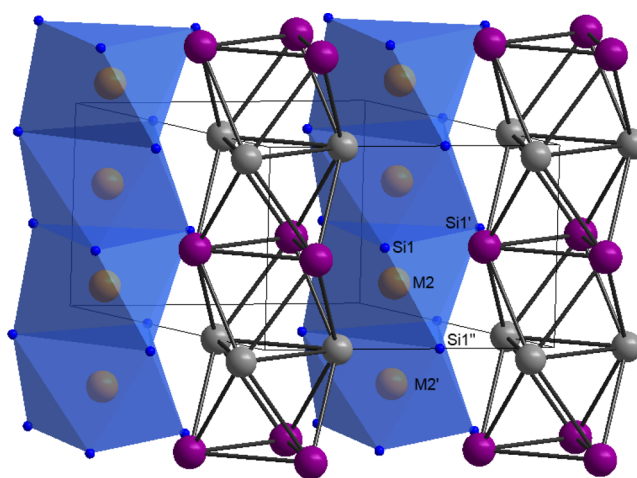


Figure 10. Projection of the structure of MnFe_4Si_3 in space group $P\bar{6}$ approximately along the $[120]$ -direction. Sites occupied by Mn and Fe are shown in magenta (M1a) and gray (M1b); sites exclusively occupied by Fe are shown in orange; Si-atoms are shown in blue. Shortest distances between M1a and M1b sites are indicated in black, and $[\text{FeSi}_6]$ -octahedra are indicated in blue. Labels of atoms correspond to the distances given in Figure 11.

the refinements is $\text{Mn}_{0.979}\text{Fe}_{4.021}\text{Si}_3$ and is thus very close to the ideal stoichiometry of MnFe_4Si_3 .

Influence of Temperature on the Structure of MnFe_4Si_3 . To characterize the influence of the temperature on the crystal structure of MnFe_4Si_3 , we collected neutron diffraction data at 380 and 200 K and a series of X-ray data sets in the temperature range from 425–200 K. Despite the response of the lattice to the magnetic transition, we do not see an indication of a change of symmetry of the structure in the whole temperature range. The X-ray data alone only allow us to refine the structure in the higher symmetrical space group $P6_3/mcm$ due to the similar contrast of Mn and Fe, yet this structure can be considered as an average structure of the lower symmetrical $P\bar{6}$ structure and thus still provides information about the structural changes.

Figure 11 shows selected interatomic distances as a function of temperature based on the refinements in $P6_3/mcm$ (absolute values of selected interatomic distances as a function of temperature are given in the Supporting Information). The only distance that clearly reflects the magnetic transition is the

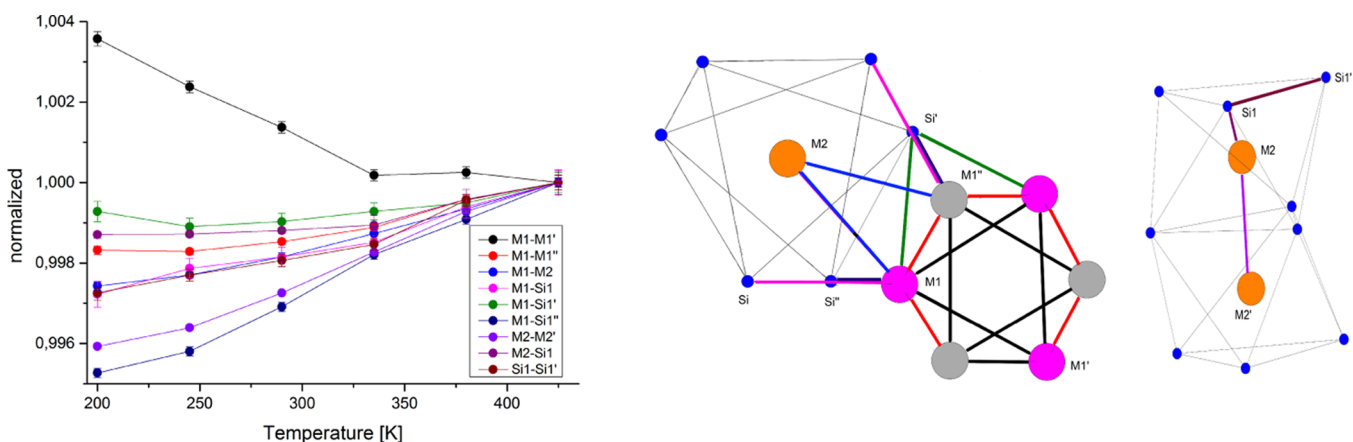


Figure 11. Left: temperature dependence of selected interatomic distances normalized to the value at 425 K obtained from X-ray single crystal diffraction. Error bars are shown if the error exceeds the size of the symbols. Right: the assignment of the distances.

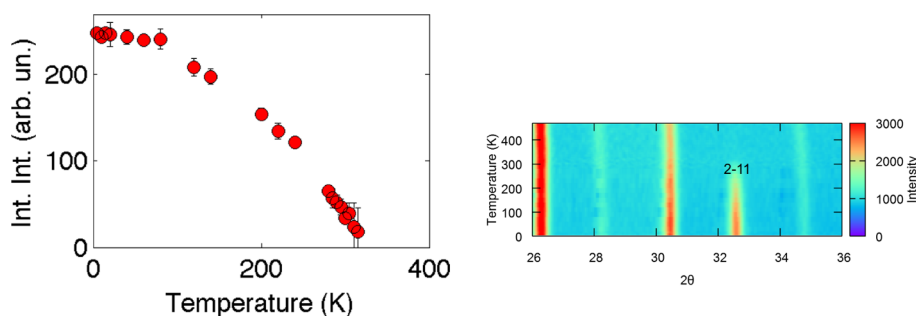


Figure 12. Integrated intensity of the $2\bar{1}1$ reflection and its symmetry equivalents obtained from Gaussian fits and the corresponding section of the neutron powder diffraction pattern as a function of temperature. The intensity of the peak increases below 300 K. Error bars are shown if the error exceeds the size of the symbols.

M1–M1' distance, which connects Mn1/Fe1 atoms of the same height parallel to the a,b -plane. This distance starts to increase significantly at the temperature corresponding to the onset of magnetic ordering (Figure 11). All other distances decrease with decreasing temperature. Distances directed along the c -axis or having a large component in this direction decrease stronger than the distances running parallel to the a,b -plane and thus mainly follow the evolution of the lattice parameter. (It is not too far to seek a hint toward the mechanism of the magnetocaloric effect in the obtained structural data, in particular in the anisotropic displacement parameters of the atoms. However, a close inspection of the temperature dependence of these parameters, as well as of the experimental electron/density, did not show any conspicuous characteristics.)

A closer look into the interatomic distances from the simultaneous refinement using both X-ray and neutron single crystal diffraction data sets for 380 and 200 K reveals more details on the interatomic distances involving the M1a and M1b sites (see table in the Supporting Information). The distance between the split atom position of Mn1a/Fe1a increases with decreasing temperature, while the distance between Mn1b/Fe1b decreases. As a general trend, both the interatomic and intraatomic distances within the $[M1a_6]$ and $[M1b_6]$ octahedra remain basically constant between atoms of the same type (Mn–Mn and Fe–Fe), yet they change between atoms of different types (Mn–Fe). The refinements also clearly show that the distorted $[M2Si_6]$ octahedra hardly change with temperature in shape and size.

Magnetic Structure of $MnFe_4Si_3$. The macroscopic magnetization measurements show a spontaneous magnetization within the a,b plane. In addition, in the neutron scattering experiments, no new reflections, which would indicate the formation of a magnetic superstructure, appear in the diffraction diagrams at 200 K. Instead, part of the reflections in the lower θ -range show an increased intensity when compared to the measurement at 380 K. This is clearly visible also in the neutron powder diffraction experiments. However, the reflection $2\bar{1}1$ and its symmetry equivalents are not observed in the diffraction patterns above the temperature at which magnetic ordering sets in, but they are clearly visible below the magnetic transition (Figure 12). The integrated intensity obtained from a Gaussian fit of the corresponding peak ($\sim 2\theta = 32.5^\circ$) is shown in Figure 12.

The above-described observations together with the results from the magnetization measurements are in agreement with ferromagnetic ordering of the spins being aligned in the a,b -plane. Of all the possible candidates of magnetic space groups, only Pm' allows for ferromagnetic ordering with the magnetic moments aligned in the a,b -plane. The refinement shows that only the M1a/M1b sites with mixed occupancies of Fe and Mn have significant magnetic moments. Their magnitude ($M_{\text{metal}} = 1.5(2)\mu_B$) is comparable in size with the effective magnetic moments per metal atom as obtained from the macroscopic measurements, even if they are obtained at an applied field, which may result in a different magnetic state, and do not reflect a fully saturated sample. The M2 sites, which are exclusively occupied by iron, yield a refined magnetic moment ($M_{M2} = 1.1(1.2)\mu_B$) not larger than the corresponding standard

deviation and were therefore not taken into account in the refinement.

The spins on the M1a/M1b sites are aligned parallel spanning an angle of $136(2)^\circ$ to the $[100]$ -direction. Between neighboring layers, the spins are ferromagnetically coupled as seen in Figure 13. The magnetic structure obtained by us is in

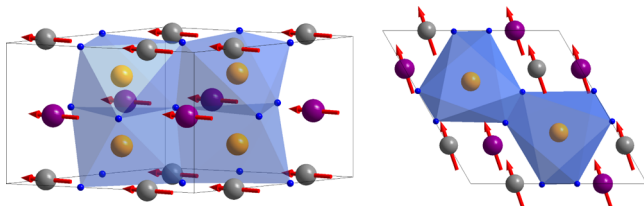


Figure 13. Schematic diagram illustrating the ferromagnetic structure of MnFe_4Si_3 at 200 K in magnetic space group Pm' . The length of the arrows corresponds to $M = 1.5(2)\mu_B$. Left, slightly tilted projection approximately along $[110]$ -direction; right, projection along $[001]$ -direction.

clear contrast to the earlier results⁵ based on neutron powder diffraction data, where the magnetic space group was chosen as $P6_3/mc'm'$, and the magnetic moments lie nearly parallel to the crystallographic c -axis with a slight tilting toward the a,b -plane. In this context, one must bear in mind that the use of single crystals both in the macroscopic magnetization measurements and in the diffraction experiment allows for a far more precise analysis of the anisotropy of the magnetization and the alignment of the spins within the crystal structure. Thus, models with an alignment of the spins both along and perpendicular to the c -direction are in accordance with powder data (it should be noted that a Rietveld refinement of our neutron powder data leads to comparable results using the two different magnetic models), yet for single crystal data only the second model explains all the observations.

According to our refinement of the magnetic structure, only the sites with mixed occupancy of Mn and Fe carry an ordered magnetic moment, while for the pure iron sites, no significant magnetic moment could be determined from the neutron single crystal data. This is in contrast to earlier Mössbauer experiments, which suggested the existence of two distinct Fe sites²³ and assumed that both the M1 and M2 sites exhibited hyperfine splitting. In this context, it is interesting to note that for iron-containing binary silicides, the absence of magnetic ordering is well-known and has been a question of debate for many years. Thus, both in FeSi and Fe_2Si , where the Fe–Si distances are comparable to the ones observed in MnFe_4Si_3 (<2.5 Å), magnetic ordering could not be clearly demonstrated,^{25–28} and it is therefore not unlikely that the long-range order of the spins on these sites is suppressed by a shielding effect by the surrounding Si-atoms not only in the Fe-silicides, but also in MnFe_4Si_3 . The discrepancy with respect to the Mössbauer investigations might result from the fact that the earlier data have always been interpreted on the basis of the structural model in $P6_3/mcm$ with two symmetrically independent Fe-atoms. Our structural model in $P6$ leads to four symmetrically independent Fe-sites and might thus require a reinterpretation of the measured Mössbauer spectra.

CONCLUSIONS

Our investigations on powder and, in particular, on single crystals of MnFe_4Si_3 provide new insight into the atomic and

magnetic structure and reveals new details that could not be obtained by studies of polycrystalline samples.

The combined use of neutron and X-ray single crystal diffraction data leads to a new structural model characterized by a partial ordering of Mn and Fe into layers perpendicular to the c -axis resulting in a reduction of the space group symmetry to $P6$. The partial ordering might be related to the fact that the atomic radius of Fe is $\sim 5\%$ smaller than the one of Mn.²⁹ It has been pointed out earlier that the preferential incorporation of Mn and Fe on different crystallographic sites in several Fe_2P -related materials³⁰ could have a strong relationship to the underlying magnetocaloric properties. It remains to be seen whether alternative synthesis strategies (e.g., slower cooling or additional tempering) could trigger a higher degree of ordering in MnFe_4Si_3 and could lead to materials with different magnetic interactions or even open ways of improving the magnetocaloric properties.

The magnetization and the magnetocaloric effect as well as the thermal expansion in MnFe_4Si_3 are strongly anisotropic. The easy axis of magnetization lies in the a,b -plane, and the spins on the Mn/Fe sites couple ferromagnetically in this plane. The occurrence of latent heat indicates the first-order character of the transition. The magnetic spacegroup is Pm' , and the sites with mixed occupancy of Mn/Fe carry an ordered magnetic moment of approximately $1.5(2)\mu_B$. Investigations of the crystal structure as a function of temperature show that most of the interatomic distances follow the trend suggested by the lattice parameter with the exception of the distance between the atoms on the sites with mixed occupancy of Mn/Fe where the observed trends are more complicated and reflect the magnetic ordering on these sites.

The presence of strong anisotropy, the preferential incorporation of different ions on different sites, and the existence of two largely independent magnetic systems might be essential ingredients for the occurrence of a large magnetocaloric effect in MnFe_4Si_3 and other compounds.

ASSOCIATED CONTENT

Supporting Information

The Supporting Information is available free of charge on the ACS Publications website at DOI: 10.1021/acs.chemmater.5b03123.

Tables of refinement results, lattice parameter, structural model, magnetic structure model, agreement factors, interatomic distances; figures of selected magnetization measurements magnetic field applied along the $[001]$ -direction and along the $[100]$ -direction (PDF) CIF files (ZIP)

AUTHOR INFORMATION

Corresponding Author

*Phone: +49 (0)02461 61 3826. Fax: +49 (0)02461 61 2610. E-mail: k.friese@fz-juelich.de.

Notes

The authors declare no competing financial interest.

ACKNOWLEDGMENTS

This work is based upon experiments performed at the SPODI instrument operated by the Karlsruhe Institute of Technology and the Technical University Munich at the Heinz Maier-Leibnitz Zentrum (MLZ), Garching, Germany, and at the TriCS Instrument operated by the Laboratory for Neutron

Scattering and Imaging at the Paul Scherrer Institute (PSI), Switzerland. We thank the referees for helpful comments.

REFERENCES

- (1) Gschneidner, K. A., Jr; Pecharsky, V. K. Thirty years of near room temperature magnetic cooling: Where we are today and future prospects. *Int. J. Refrig.* **2008**, *31*, 945–961.
- (2) Tegus, O.; Brueck, E.; Buschow, K. H. J.; de Boer, R. R. Transition-metal-based magnetic refrigerants for room-temperature applications. *Nature* **2002**, *415*, 150–152.
- (3) Candini, A.; Moze, O.; Kockelmann, W.; Cadogan, J. M.; Brueck, E.; Tegus, O. Revised magnetic phase diagram for $\text{Fe}_x\text{Mn}_{5-x}\text{Si}_3$ intermetallics. *J. Appl. Phys.* **2004**, *95*, 6819–6821.
- (4) Binczycka, H.; Dimirijevic, Z.; Gajic, B.; Szytula, A. Atomic and Magnetic Structure of $\text{Mn}_{5-x}\text{Fe}_x\text{Si}_3$. *Phys. stat. sol.* **1973**, *19*, K13–K17.
- (5) Gourdon, O.; Gottschlich, M.; Persson, J.; de la Cruz, C.; Petricek, V.; McGuire, M. A.; Brückel, T. Toward a better understanding of the magnetocaloric effect: An experimental and theoretical study of MnFe_4Si_3 . *J. Solid State Chem.* **2014**, *216*, 56–64.
- (6) Gottschlich, M.; Gourdon, O.; Persson, J.; de la Cruz, C.; Petricek, V.; Brückel, T. Study of the antiferromagnetism of Mn_5Si_3 : an inverse magnetocaloric effect material. *J. Mater. Chem.* **2012**, *22*, 15275–15284.
- (7) Songlin; Dagula; Tegus, O.; Brueck, E.; Klaasse, J. C. P.; de Boer, F. R.; Buschow, K. H. J. Magnetic phase transition and magnetocaloric effect in $\text{Mn}_{5-x}\text{Fe}_x\text{Si}_3$. *J. Alloys Compd.* **2002**, *334*, 249–252.
- (8) Pecharsky, V. K.; Gschneidner, K. A., Jr Giant Magnetocaloric Effect in $\text{Gd}_5(\text{Si}_2\text{Ge}_2)$. *Phys. Rev. Lett.* **1997**, *78*, 4494–4497.
- (9) Gschneidner, K. A., Jr; Pecharsky, V. K.; Tsokol, A. O. Recent developments in magnetocaloric materials. *Rep. Prog. Phys.* **2005**, *68*, 1479–1539.
- (10) Gier, H. *Kalt-Schmelz-Tiegel*. Eur. Pat. EP 0 345542 B1, 1993.
- (11) Wilke, K.-T. *Kristallzuechtung*; VEB Deutscher Verlag der Wissenschaften: Berlin, 1973.
- (12) Hoelzel, M.; Senyshyn, A.; Juenke, N.; Boysen, H.; Schmahl, W.; Fuess, H. High-resolution neutron powder diffractometer SPODI at research reactor FRM II. *Nucl. Instrum. Methods Phys. Res., Sect. A* **2012**, *667*, 32–37.
- (13) Data collection and data reduction GUI: Agilent Technologies. *CrysAlisPro 171.36.28*, 2012.
- (14) STOE & Cie GmbH. *X-SHAPE Version 2.07*, 2005.
- (15) Schefer, J.; Könnicke, M.; Murasik, A.; Czopnik, A.; Strässle, T.; Keller, P.; Schlumpf, N. Single-crystal diffraction instrument TriCS at SINQ. *Phys. B* **2000**, *276-278*, 168–169.
- (16) LeBail, A.; Duroy, H.; Fourquet, J. L. Ab-initio structure determination of LiSbWO_6 by X-Ray powder diffraction. *Mater. Res. Bull.* **1988**, *23*, 447–452.
- (17) Crystallographic computing system for standard and modulated structures: Petricek, V.; Dusek, M.; Palatinus, L. *Jana2006 Version 30/11/2014*, 2006.
- (18) Howard, C. J. The approximation of asymmetric neutron powder diffraction peaks by sums of Gaussians. *J. Appl. Crystallogr.* **1982**, *15*, 615–620.
- (19) Ivantchev, S.; Kroumova, E.; Madariaga, G.; Perez-Mato, J. M.; Aroyo, M. I. SUBGROUPGRAPH: a computer program for analysis of group-subgroup relations between space groups. *J. Appl. Crystallogr.* **2000**, *33*, 1190–1191.
- (20) Hamilton, W. C. Significance tests on the crystallographic R factor. *Acta Crystallogr.* **1965**, *18*, 502–510.
- (21) Petricek, V.; Dusek, M.; Fuksa, J. Magnetic space and superspace groups, representation analysis: competing or friendly concepts? *Acta Crystallogr., Sect. A: Found. Crystallogr.* **2010**, *66*, 649–655.
- (22) Caron, L.; Ou, Z. Q.; Nguyen, T. T.; Cam Thanh, D. T.; Tegus, O.; Brueck, E. On the determination of the magnetic entropy change in materials with first-order transitions. *J. Magn. Magn. Mater.* **2009**, *321*, 3559–3566.
- (23) Narasimhan, K. S. V. L.; Reiff, W. M.; Steinfink, H.; Collins, R. I. Magnetism and bonding in a D_{8h} structure; Mössbauer and magnetic investigation of the system $\text{Mn}_5\text{Si}_3\text{-Fe}_5\text{Si}_3$. *J. Phys. Chem. Solids* **1970**, *31*, 1511–1524.
- (24) Wohlfarth, E. P. Magnetic properties of crystalline and amorphous alloys: A systematic discussion based on the Rhodes-Wohlfarth plot. *J. Magn. Magn. Mater.* **1978**, *7*, 113–120.
- (25) Misawa, S.; Tate, A. Fermi liquid description of the anomalous magnetic susceptibility of FeSi. *J. Magn. Magn. Mater.* **1996**, *157-158*, 617–618.
- (26) Kubaschewski, O. *Iron-Binary Phase Diagrams*; Springer: New York, 1982.
- (27) Watanabe, H.; Yamamoto, H.; Ito, K. Neutron Diffraction Study of the Intermetallic Compound FeSi. *J. Phys. Soc. Jpn.* **1963**, *18*, 995–999.
- (28) Shirane, G.; Fischer, J. E.; Endoh, Y.; Tajima, K. Temperature-induced magnetism in FeSi. *Phys. Rev. Lett.* **1987**, *59*, 351–354.
- (29) Cordero, B.; Gomez, V.; Platero-Prats, A.; Reves, M.; Echeverria, J.; Cremades, E.; Barragan, F.; Alvarez, S. Covalent radii revisited. *Dalton Transactions* **2008**, 2832–2838.
- (30) Neish, M. J.; Oxley, M. P.; Guo, J.; Sales, B. C.; Allen, L. J.; Chisholm, M. F. Local Observation of the Site Occupancy of Mn in a MnFePSi Compound. *Phys. Rev. Lett.* **2015**, *114*, 106101.